



OPEN Identification of metabolic pathways and serum biomarkers in diabetic cardiomyopathy using untargeted metabolomics

Jialong Li^{1,2}, Huaming Qiu^{3,4}, Yanjun Wu³ & Li Su¹✉

Diabetic cardiomyopathy represents a significant and irreversible chronic cardiovascular complication among diabetic patients. The condition is characterised by early diastolic dysfunction, myocardial fibrosis, cardiac hypertrophy, systolic dysfunction, and other complex pathophysiological events that ultimately lead to heart failure. Untargeted metabolomic analysis represents a powerful tool for the discovery of novel biomarkers. It can not only reveal the metabolic disorder model of diabetic cardiomyopathy, and find specific biomarkers, but also help analyse its pathogenesis and provide new clues for developing treatment strategies. Nevertheless, the precise mechanisms that give rise to diabetic cardiomyopathy remain unclear. In this study, we established a rat model of diabetic cardiomyopathy. We evaluated the model using various established methods, including fasting glucose, glycated hemoglobin, insulin resistance index, cardiac histopathology, and cardiac ultrasound. We then proceeded to identify diabetic cardiomyopathy serum biomarkers by untargeted metabolomics. The potential metabolic pathways of the multiple metabolic differentials were mainly related to amino acid metabolism and arachidonic acid metabolism. Two common metabolites, 5-OxoETE and D-Glutamine, were identified through various cross-comparisons. These two metabolites have good diagnostic ability, especially between DCM vs. CTR, DCM vs. NDCM, and NDCM vs. CTR. These findings may provide new insights into the study of DCM.

Keywords Diabetic cardiomyopathy, Untargeted metabolomics, Cardiac ultrasound, Ejection fraction, Diagnostic biomarkers

The global prevalence of diabetes mellitus (DM) is increasing annually, with projections indicating that the number of individuals with DM will reach 578.4 million by 2030¹. With the increasing prevalence of diabetes, the burden of diabetes and its complications, including cardiomyopathy, is increasing worldwide. Diabetic cardiomyopathy is a kind of myocardial disease. The difference between diabetic cardiomyopathy and other heart diseases (including hypertensive heart disease, coronary atherosclerotic heart disease, and heart valve disease) is the long-term existence of hyperglycemia². The incidence rate of diabetic cardiomyopathy is relatively high in diabetes patients. Some studies have shown that the prevalence of diabetic cardiomyopathy is about 30–60%³. Diabetic cardiomyopathy is one of the serious complications of diabetes and one of the most common causes of death in patients with diabetes^{4,5}.

The pathogenesis of diabetic cardiomyopathy may be attributed to several factors, including metabolic disorders in cardiomyocytes⁶, myocardial cell calcium transport defects⁷, microangiopathy of the coronary arteries⁸, myocardial interstitial fibrosis⁹, an inflammatory response¹⁰, and oxidative stress¹¹. Long-term insulin resistance not only results in a hyperglycaemic state, which impairs mitochondrial function in cardiomyocytes and generates a large number of free radicals and ROS, consequently leading to myocardial energy metabolism disorders and oxidative stress reactions but also causes excessive oxidation of fatty acids in cardiomyocytes, which leads to the accumulation of triglycerides and free fatty acids in cardiomyocytes, thus affecting the diastolic and contractile functions of the heart¹². Prolonged hyperglycaemia has been demonstrated to cause inhibition of sodium-calcium exchange in cardiomyocytes, resulting in a gradual concentration of Ca²⁺ in the

¹Department of Cardiology, The Second Affiliated Hospital, Chongqing Medical University, Chongqing, China.

²Department of Cardiovascular Medicine, The Affiliated Hospital of Sichuan Nursing Vocational College, The Third People's Hospital of Sichuan Province, Sichuan Province Chengdu, China. ³Guizhou University of Traditional Chinese Medicine, Guizhou Guiyang, China. ⁴Department of Acupuncture and moxibustion, Pengzhou Hospital of Traditional Chinese Medicine, Sichuan Province Chengdu, China. ✉email: sulicq@hospital.cqmu.edu.cn

sarcoplasmic reticulum. An overload of Ca^{2+} in the cardiac sarcoplasmic reticulum may increase the release of spontaneous Ca^{2+} . Abnormal changes in the concentration of intracellular calcium ions in the cardiomyocyte may lead to pathological alterations, including cardiomyocyte hypertrophy, degeneration, focal necrosis, and other pathological changes¹³. In patients with diabetes, the myocardium displays extensive diffuse intramural microangiopathy, which can result in a diminished reactivity of the myocardial microvasculature to vasoactive substances (e.g., angiotensin, nitric oxide). This, in turn, leads to a substantial reduction in the reserve function of coronary arteries, which ultimately gives rise to extensive myocardial ischemia, degeneration, necrosis, and fibrosis¹⁴. While the factors mentioned above contribute to the pathogenesis of diabetic cardiomyopathy, they remain insufficiently elucidated.

Metabolomics can provide new insights into the complex biochemical processes underlying disease by systematically investigating organism metabolite composition, content, and level changes^{15,16}. Non-targeted metabolomics refers to the use of techniques such as liquid chromatography-mass spectrometry (LC-MS), gas chromatography-mass spectrometry (GC-MS), and nuclear magnetic resonance (NMR) to detect the dynamic changes of all small molecule metabolites before and after stimulation or disturbance in cells, tissues, organs, or organisms without bias. They screen differential metabolites through bioinformatics analysis and conduct pathway analysis on these differential metabolites to reveal their physiological mechanisms of change. Therefore, metabolomics offers a promising avenue for advancing our understanding of the pathogenesis of T2DM and its complications^{17,18}. The application of metabolomic techniques has been demonstrated to facilitate comprehension of the intricate interrelationships between metabolic dysfunction, diabetes, and cardiac function¹⁹. By concentrating on metabolic dysfunction, and biomarkers, and identifying specific metabolic pathways, metabolomic investigations can offer a new direction for us to find the markers and potential therapeutic targets of diabetic cardiomyopathy²⁰.

Materials and methods

Laboratory animal

All procedures were approved by the Experimental Animal Management and Use Committee of the Second Affiliated Hospital of Chongqing Medical University (No. IACUC-SAHCOMU-2024-00016). All experiments were conducted by the Laboratory Animal—Guideline for Ethical Review of Animal Welfare issued by the Chinese Technical Committee for Standardization of Laboratory Animals and General Administration of Quality Supervision, Inspection and Quarantine of the People's Republic of China (Standard NO: GB/T 35892 – 2018). This study was carried out in compliance with the ARRIVE guidelines. Seventy-five male pathogen-free (SPF) Sprague Dawley (SD) rats (weight = 315 ± 25 g) were purchased from Beijing Vital River Laboratory Animal Technology Co., Ltd. (Beijing, China; License No.: SCXK (Jing) 2021-0006). They were kept in the SPF Laboratory Animal Center, The Second Affiliated Hospital of Chongqing Medical University (Laboratory Animal License No.: SYXK (Yu) 2023-0005). The laboratory animal room was maintained at a suitable temperature ($23 \pm 3^\circ\text{C}$), the humidity was controlled at $60\% \pm 5\%$, in a standard cage, each batch of 5 rats was raised in a cage, free food and water, natural lighting, and the law of day and night, light and dark cycle was 12 h/12 h.

Reagents and materials

The streptozotocin was provided by Beijing Solarbio Science&Technology Co., Ltd. (Beijing, China, batch: 24240306011). The 0.1 mol/L sodium citrate buffer was supplied by Beijing Solarbio Science&Technology Co., Ltd. (Beijing, China, batch: 240002002). The 4% paraformaldehyde tissue fixative was purchased from Biosharp (24109404), while the 2.5% glutaraldehyde fixative was purchased from the same supplier (BL911 A). Isoflurane was purchased from RWD Life Science Co., Ltd. (model: R510-22-10). The Roche blood glucose meter (ACCU-CHEK Guide) was procured from Roche Diagnostics GmbH, a company based in Germany. The Glycated hemoglobin A1c (GHbA1c) enzyme-linked immunosorbent assay (ELISA) kit was procured from ShangHai CHUTAI Biology Science and Technology Co., Ltd. (China; batch number: 202406). The Rat Fasting Insulin (FINS) ELISA kit was procured from ShangHai CHUTAI Biology Science and Technology Co., Ltd. (China; batch number: 202406). The auto chemistry analyser was procured from Rayto Life and Analytical Sciences Co., Ltd. bearing the batch numbers Chemray 240 and Chemray 420.

DCM modelling approach

After one week of adaptive feeding, the rat was randomly divided into 2 groups as follows: the normal control group (CTR, $n = 15$) and the streptozotocin group (STZ, $n = 60$). The normal control group was provided with a standard maintenance diet. The streptozotocin group was provided with a fat and high-sugar diet. After 4 weeks of feeding, the streptozotocin group was intraperitoneally injected with streptozotocin (STZ) (35 mg/Kg)²¹ 12 h after fasting, while the normal control group was intraperitoneally injected with the same volume of 0.1 mol/L sodium citrate buffer 12 h after fasting. After one week, the streptozotocin group with fasting blood glucose (FBG) levels $> 14 \text{ mmol/L}$ were selected as diabetic rats and 39 diabetic rats were obtained (39 of 60 rats, 15 died, 6 were not modelled, 65%)^{22,23}. The diabetes model group continued to feed high fat and high-sugar diet. Perform echocardiography at weeks 11 and 12. Rats in the diabetes model group with ejection fraction (EF) $< 50\%$ for two consecutive times were included in the diabetes cardiomyopathy group (DCM group), and rats in the diabetes model group with EF $> 50\%$ for two straight times were included in the non-diabetes cardiomyopathy group^{24,25}.

Model evaluation metrics and methods

Model success criteria

(1) Weight shows a trend of first increasing and then decreasing, while water intake, diet, and urine output show a continuously increasing trend; (2) Fasting blood glucose is greater than 14.0 mmol/L ; (3) Biochemical indicators

include elevated glycated hemoglobin, elevated blood lipids, and insulin resistance; (4) Histopathological manifestations include myocardial cell damage and pancreatic islet cell destruction; (5) Cardiac ultrasound shows that the EF value is less than 50% in two consecutive measurements.

The model assessment was performed as follows

General observation

Body weight, diet, water intake, and 24-hour urine output were observed and recorded for three animal groups.

Assessment of diabetes

One week after the intraperitoneal injection of STZ, blood glucose was measured 12 h after fasting. Following the sterilisation of the tail tip of the rats with medical alcohol, blood was collected by piercing the tail tip with a blood collection needle, and the change in fasting blood glucose (FBG) was determined and recorded. The establishment of a fasting blood glucose level exceeding 14 mmol/L in the diabetes model group was deemed indicative of successful diabetes modelling. Subsequently, the fasting blood glucose of the three groups was evaluated at a fixed time point every week.

Enzyme-linked immunosorbent assay (ELISA): Blood is collected from the abdominal aorta of rats and allowed to solidify naturally for 10–20 min at room temperature. The blood is centrifuged for approximately 10 min at 3000 rpm. The supernatant was then meticulously collected. Glycosylated hemoglobin and fasting insulin levels in rat serum were measured according to the method described in the instructions of the ELISA kit. Insulin resistance (IR) was measured via homeostatic model assessment (HOMA-IR), where the HOMA-IR score = $\text{FBG} \times \text{INS} / 22.5^{26}$.

Detection of blood lipids

Blood samples were extracted from the abdominal aorta of rats, and the supernatant was subjected to centrifugation. After that, the TG, CHO, HDL and LDL levels were determined using the auto chemistry analyser (Rayto Life and Analytical Sciences Co., Ltd, Shenzhen, China).

Cardiac echocardiography measurement

Following inhalation anaesthesia with isoflurane, the experimental rats were fixed supine on the experimental fixation plate. All rats underwent echocardiographic examinations using an ultrasound system (6LAB; Vinno Technology, China) via an X6-16 L probe (14 MHz). All measurements were performed according to the American Society of Echocardiography guidelines. The values of left ventricular internal diameter at end-diastole (LVIDd), and left ventricular internal diameter at end-systole (LVIDs) were recorded in M-mode ultrasound mode. At least three consecutive cardiac cycles were observed in each rat, and the mean values were calculated. The LVEF and left ventricular diameter shortening rate (LVFS) were calculated by Teichholz²⁷.

Cardiac pathology (Hematoxylin-eosin staining, Masson's trichrome staining)

At the end of the experiment, the rats were euthanised using carbon dioxide and samples were collected.

Hematoxylin-eosin staining (HE): Hearts and pancreas samples were quickly extracted from each of the 3 groups of rats and then fixed in 4% paraformaldehyde overnight. Hearts and pancreas were then dehydrated with graded alcohol and embedded in paraffin. The 5 µm thick paraffin-embedded myocardial tissue and pancreatic tissue sections were then processed with the HE kit to observe the pathological changes in the myocardial tissue and pancreatic tissues.

Masson's trichrome staining: The heart tissue of three groups of rats was rapidly extracted and fixed in 4% paraformaldehyde. Once the fixation process is complete, strictly follow the SOP procedure for pathological experimental examination to trim, dehydrate, embed, slice, stain, and seal the sample, and finally examine microscopically to ensure the quality of the samples. The target area of the tissue should be selected for 200x imaging using the Eclipse Ci-L photo microscope. When imaging, try to make the tissue full of the whole field of vision to ensure that the background light of each photo is consistent. After imaging, use the Image-Pro Plus 6.0 processing system to calculate the myocardial collagen score in each field of view of the slice (CVF = collagen area in the same image/measured field of view area). Randomly select 3 fields of view for each slice to take photos, and take the average as the number, excluding collagen-rich blood vessels and scarred areas.

Untargeted metabolomics analysis

Sample pretreatment

Approximately 5 mL of blood was collected from each rat into a blood collection tube, followed by centrifugation. The resulting serum was transferred to a frozen pipe and stored in a −80 °C refrigerator. Each group of six serum samples were thawed gradually at 4 °C. The samples (100 µL) were placed in the EP tubes and suspended with resuspended with prechilled 400 µL of 80% methanol by well vortex. The samples were incubated on ice for 5 min and centrifuged at 15,000 g, 4 °C for 20 min. A certain amount of the supernatant was diluted with LC-MS grade water until the methanol content was 53%. The supernatant was collected by centrifugation at 15,000 g, 4 °C for 20 min, injecting the sample and performing LC-MS analysis.

Acquisition conditions for chromatography and mass spectrometry

Perform chromatographic separation using HypersilGoldcolumn C18 chromatographic column. The column temperature was 40 °C and the flow rate was 0.2 mL/min. The eluents for the positive and negative polarity modes were eluent A (0.1% FA in Water) and eluent B (Methanol). The mobile phase A was water containing 0.1% formic acid, while the mobile phase B was methanol. The metabolites were eluted using the following

gradients: 0–1.5 min, 98% A, 2% B; 1.5–3.0 min, 15% A, 85% B; 3.0–10.0 min, 100% B; 10.0–12.0 min, 98% A, 2% B. Mass spectrometer was operated in positive/negative polarity mode with spray voltage of 3.5 kV, capillary temperature of 320 °C, sheath gas flow rate of 35 psi and aux gas flow rate of 10 L/min, S-lens RF level of 60, Aux gas heater temperature of 350 °C. The injection volume for each sample was 5 µL. Throughout the analysis process, the sample was kept in an automatic sampler at 4 °C. To avoid any influence of instrument signal fluctuations, the samples were analysed in a randomised sequence. Quality control (QC) samples were introduced after each set of samples in the sample queue to monitor and evaluate the stability of the system and the reliability of experimental data.

Data preprocessing and analysis

The raw data files generated by UHPLC-MS/MS were processed using Compound Discoverer 3.3 (CD3.3, ThermoFisher) to perform peak alignment, peak picking, and quantitation for each metabolite. The main parameters were set as follows: peak area was corrected with the first QC, actual mass tolerance, 5ppm; signal intensity tolerance, 30%; and minimum intensity, et al. After that, peak intensities were normalized to the total spectral intensity. The normalized data was used to predict the molecular formula based on additive ions, molecular ion peaks and fragment ions. Then peaks were matched with the mzCloud (<https://www.mzcloud.org/>), mzVault and MassList databases to obtain accurate qualitative and relative quantitative results.

The unsupervised model (principal component analysis, PCA) was used to elucidate the intrinsic similarities and differences between the various samples. Using the supervised model of partial least squares discriminant analysis (PLS-DA), subtle and minor differences in the metabolic phenotypes of the various samples were better captured. The fitting ability (R²_Y) and predictability (Q²) of the models provided evidence of the quality of the various PLS-DA models obtained. The variable importance in projection (VIP) values from the PLS-DA models helped to identify metabolites with significant contributions to the group classifications (i.e., differential metabolites). Principal components analysis (PCA) and Partial least squares discriminant analysis (PLS-DA) were performed at metaX (a flexible and comprehensive software for processing metabolomics data). Metabolite set enrichment analysis was conducted based on the differentially expressed metabolites using MetaboAnalyst 6.0 (<http://www.metaboanalyst.ca>).

A receiver operating characteristic (ROC) analysis was performed in MetaboAnalyst 6.0 (<http://www.metaboanalyst.ca/>), to calculate the area under curve (AUC). Optimal cutoffs were shown using the “closest to top-left corner” method. In general, an area under the ROC curve between 0.5 and 0.7 was indicative of a low diagnostic value, between 0.7 and 0.9 was indicative of a moderate diagnostic value, and above 0.9 was indicative of a high diagnostic value.

Statistical analysis

Statistical analysis was conducted using SPSS 26.0 software and GraphPad Prism 9.5 software for data visualization. For data that follows a normal distribution and demonstrates homogeneity of variance, one-way analysis of variance (ANOVA) was utilized to compare multiple groups. Post hoc pairwise comparisons between multiple groups were performed using the Bonferroni. Data is presented as the mean ± standard deviation, with statistical significance defined as $p < 0.05$.

Results

The main indicators of laboratory animals are as follows

The following parameters were assessed: body weight, diet, water intake, 24-hour urine output, fasting blood glucose, glycosylated hemoglobin, insulin resistance index, blood lipids, cardiac echocardiography, and cardiac pathology (Hematoxylin-eosin staining, Masson's trichrome staining).

The general condition of rats

During the modelling process, 39 diabetes model group (DM) rats were finally obtained (39 of 60, 15 died, 6 were not modelled, 65%). The final DCM model consisted of 9 rats, the NDCM model consisted of 30 rats, and the CTR group consisted of 15 rats. By the conclusion of the fourth week, the body weight of both the NDCM and DCM groups had increased significantly in comparison to the CTR group ($P < 0.01$). Following the administration of intraperitoneal injection of STZ-induced diabetes, the body weights of the NDCM and DCM groups exhibited a notable decline relative to the CTR group at the sixth, eighth, tenth, and twelfth weeks, indicating a downward trend in body weight (Fig. 1A). The diet (Fig. 1C), water intake (Fig. 1B), and 24-hour urine output (Fig. 1D) of the NDCM and DCM groups were significantly higher than that of the CTR group ($P < 0.01$). No statistical difference was observed between the NDCM and DCM groups in the body weight, diet, water intake and 24-hour urine output.

Diagnostic indicators of diabetes in rats

NO statistical change was observed in fasting blood glucose levels in the three groups of rats in the fourth week. Following the intraperitoneal injection of STZ-induced diabetes, the fasting blood glucose of the NDCM and DCM groups was significantly higher than that of the CTR group at the sixth, eighth, tenth, and twelfth weeks ($P < 0.01$). This was accompanied by a rapidly rising trend from weeks four to eight and a stable trend from weeks eight to twelve (Fig. 1E). The Glycosylated hemoglobin (Fig. 1F) and insulin resistance index (Fig. 1G) of the NDCM and DCM groups were significantly higher than that of the CTR group ($P < 0.01$). No statistical difference was observed between the NDCM and DCM groups at the fasting blood glucose, the Glycosylated hemoglobin and insulin resistance index.

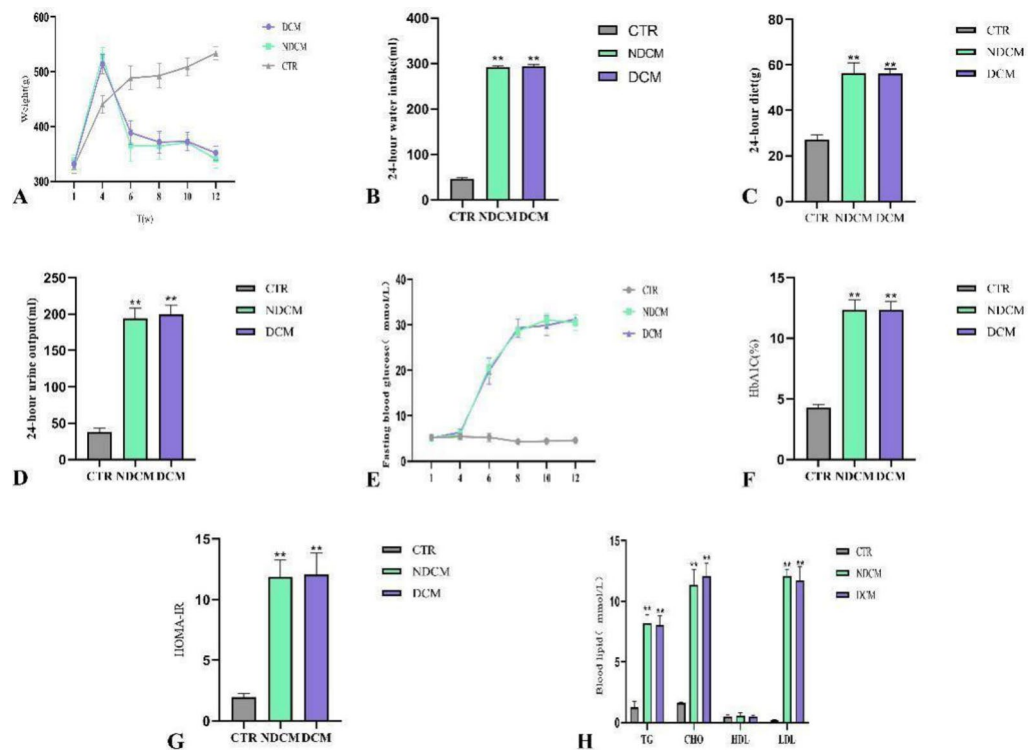


Fig. 1. The body weight, water intake, diet, urine output, fasting blood glucose, serum glycated hemoglobin, insulin resistance index, and blood lipids of each group of rats (CTR, NDCM, DCM) are shown in the figure. Among them, A is the weight of each group of rats, B is the 24-hour water intake of each group of rats, C is the 24-hour dietary intake of each group of rats, D is the 24-hour urine output of each group of rats, E is the fasting blood glucose of each group of rats at weeks 1, 4, 6, 8, 10, and 12, F is the serum glycated hemoglobin of each group of rats, G is the insulin resistance index of each group of rats, and H is the TG, CHO, HDL, LDL of each group of rats.

Blood lipids in rats

The TG, CHO and LDL levels were found to be significantly elevated in the NDCM and DCM groups compared to the CTR group ($P < 0.01$). No statistical differences were observed between the two groups within the NDCM and DCM groups at the TG, CHO and LDL. No statistical differences were observed in HDL levels between the three groups (Fig. 1H).

Cardiac echocardiography

The EF (Fig. 2A) and FS (Fig. 2B) in the DCM group were found to be significantly lower than those in the NDCM and CTR groups ($P < 0.01$). No statistical differences were observed between the two groups within the NDCM and CTR groups at the EF and FS. Similarly, the LVIDd (Fig. 2C) and LVIDs (Fig. 2D) in the DCM group were found to be significantly higher than those in the NDCM and CTR groups ($P < 0.01$). No statistical differences were observed between the two groups within the NDCM and CTR groups at the LVIDd and LVIDs.

Pancreatic pathology

The pancreatic tissues of rats in the CTR (Fig. 3A and B) group exhibited uniform staining, and the acinar cells were normal in morphology and structure, regular in shape, without obvious inflammation. The NDCM (Fig. 3C and D) and DCM (Fig. 3E and F) groups exhibited notable pathological alterations, including a small number of islets, different sizes, interstitial oedema, the cytoplasm of pancreatic islet cells displaying looseness, degeneration of acinar cells, lymphocyte infiltration, and invasion of acinar cells into the islets.

Cardiac pathology (Hematoxylin-eosin staining, Masson's trichrome staining)

Hematoxylin-eosin staining: The endocardium, myocardium and epicardium of the heart tissue of rats in the CTR (Fig. 3G) group exhibited a clear structural organisation, with cardiomyocytes arranged in a tightly packed configuration, delineated by distinct cellular boundaries and exhibiting a consistent orientation. In comparison to the CTR group, the cardiomyocytes of rats in the NDCM (Fig. 3I) and DCM (Fig. 3K) groups exhibited oedema, sparse and light staining of the cytoplasm, and a proliferation of connective tissues within the endocardium and mesenchyme, accompanied by punctiform infiltration of fibroblasts and lymphocytes.

Masson's trichrome staining: The CTR group have intact myocardial tissue structure, clear cell nuclei, tightly and regularly arranged myocardial fibres and no obvious collagen deposition (Fig. 3H). Part of the myocardial cells in the NDCM group showed oedema, increased intercellular space, a partial disorder of myocardial fibres,

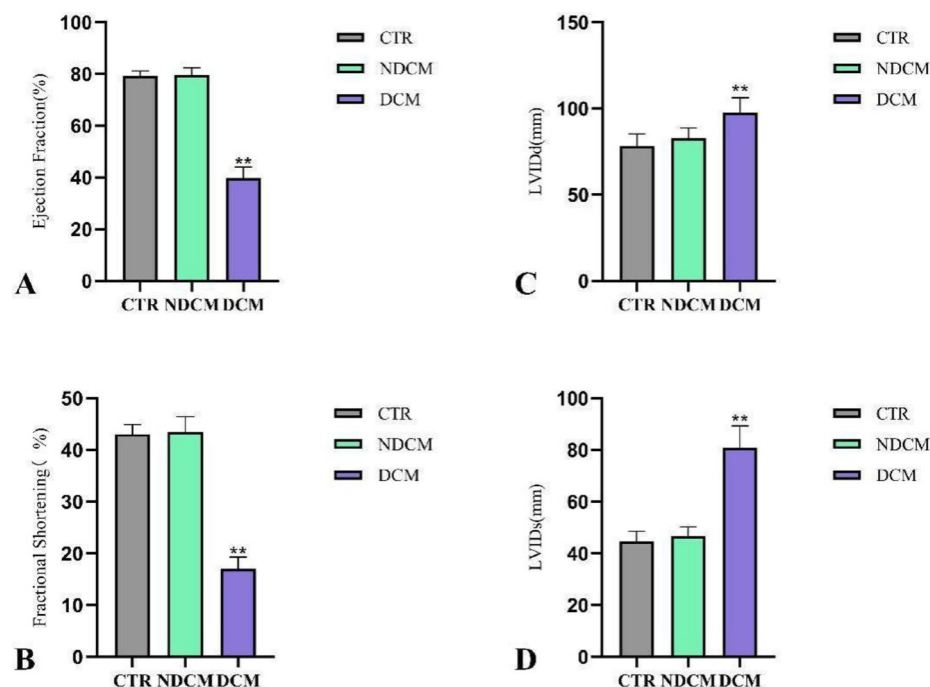


Fig. 2. The EF, FS, LVIDd, and LVIDs of each group of rats (CTR, NDCM, DCM) are shown in the figure. Among them, A is the EF of each group of rats, B is the FS of each group of rats, C is the LVIDd of each group of rats, and D is the LVIDs of each group of rats.

and accumulation of collagen fibres (Fig. 3J). The myocardial cells of the DCM group showed oedema, increased intercellular space, disordered myocardial fibres, and collagen fibre accumulation (Fig. 3L). Collagen area fraction results (Fig. 3M): The myocardial collagen area fraction was significantly higher in the NDCM and DCM groups when compared with the CTR group ($P < 0.01$). No statistical differences were observed between the two groups within the NDCM and DCM groups at collagen area fraction results.

Metabolomics

Comparison of overall metabolome analysis and differential metabolite

The metabolomic phenotypes from the various cross-comparisons have been summarized in Fig. 4. A visual analysis of Fig. 4 exposes the metabolic features of the unsupervised PCA model in discriminating between the various metabolic phenotypes. There is an overlap in the metabolic features from the various comparisons using the PCA model. These apparent phenotypic similarities were however clearly distinguished using the supervised PLS-DA model with good fitting (R^2Y) and predictive abilities (Q^2). From the 3 cross-comparisons and using the selection criterion earlier highlighted, various differential metabolites were identified. As illustrated in the accompanying figure (Fig. 4).

Differential metabolites

From three cross-comparisons of DCM. vs. CTR, NDCM. vs. CTR, and DCM. vs. NDCM, and using the selection criteria emphasised earlier, various differential metabolites were identified. A total of 210 metabolites were identified in the POS mode of the DCM. vs. CTR comparison, of which 149 were up-regulated and 61 were down-regulated. Similarly, a total of 147 metabolites were identified in the NEG mode of the DCM. vs. CTR comparison, of which 104 were up-regulated and 43 were down-regulated. A total of 297 metabolites were identified in the POS mode of the NDCM. vs. CTR comparison, of which 132 were up-regulated and 165 were down-regulated. Similarly, a total of 218 metabolites were identified in the NEG mode of the NDCM. vs. CTR comparison, of which 108 were up-regulated and 110 were down-regulated. A total of 209 metabolites were identified in the POS mode of the DCM. vs. NDCM comparison, of which 136 were up-regulated and 73 were down-regulated. Similarly, a total of 175 metabolites were identified in the NEG mode of the DCM. vs. NDCM comparison, of which 100 were up-regulated and 75 were down-regulated. All the above results are displayed in the heatmap (Fig. 5).

Metabolic pathways of potential disorders

Several related metabolic pathways were identified as relevant based on the differential metabolites that were identified from the DCM group compared to the CTR group. As illustrated (Fig. 6A, B), the disorganized metabolic pathways include aldosterone synthesis and secretion, bile secretion, valine, leucine and isoleucine degradation, propanoate metabolism, riboflavin metabolism, lysine degradation, vitamin digestion and absorption, arginine and proline metabolism, ABC transporters, 2-oxo carboxylic acid metabolism, pentose

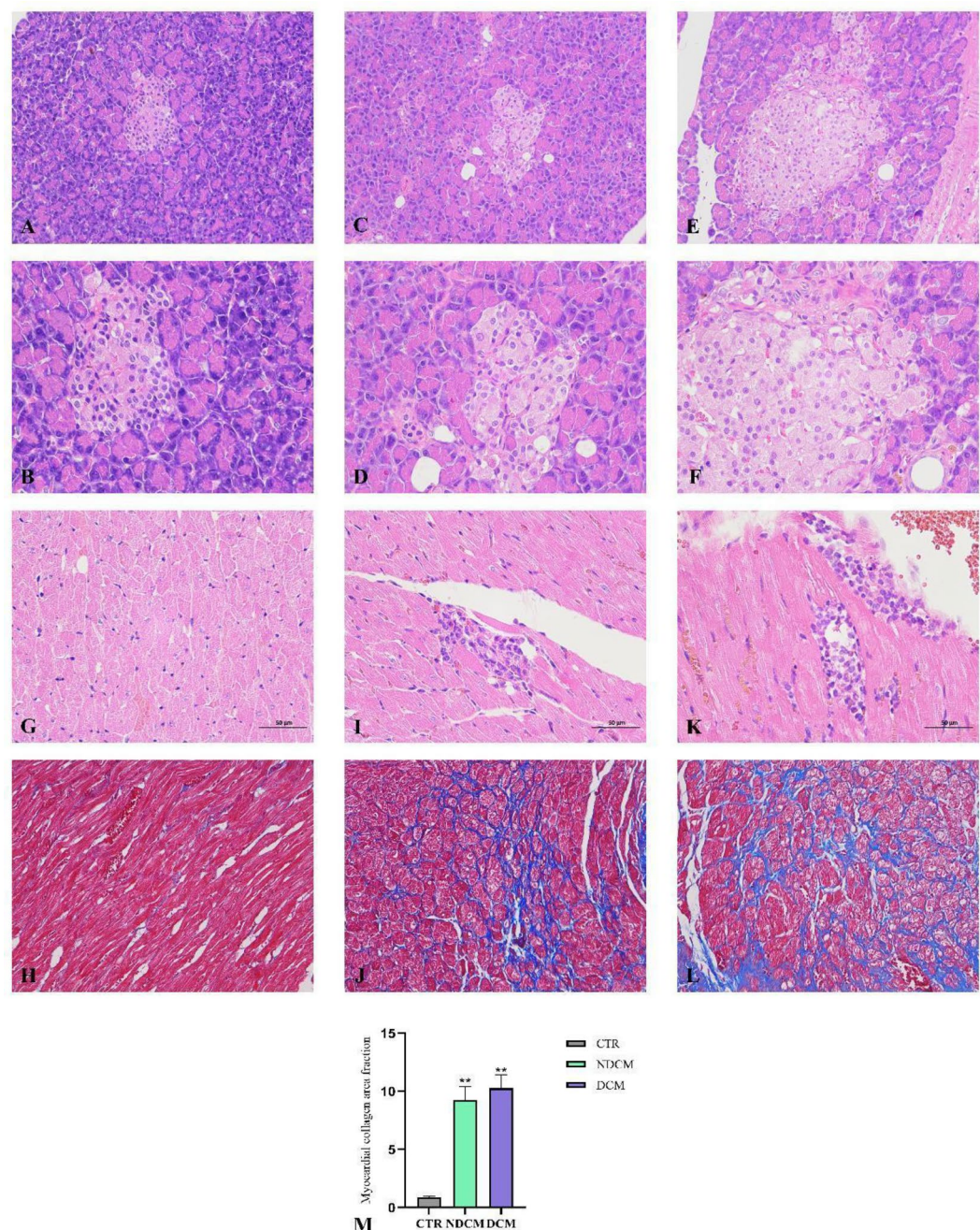


Fig. 3. The pancreatic HE histopathology of each group of rats (CTR, NDCM, DCM) is shown in the figure. Among them, A is the HE200 fold of pancreas in CTR group rats, B is the HE400 fold of pancreas in CTR group rats, C is the HE200 fold of pancreas in NDCM group rats, D is the HE400 fold of pancreas in NDCM group rats, E is the HE200 fold of pancreas in DCM group rats, and F is the HE400 fold of pancreas in DCM group rats. The cardiac HE and Masson staining histopathology of each group of rats (CTR, NDCM, DCM) are also shown in the figure. Among them, G is the heart muscle HE400 times of the CTR group rats, H is the heart muscle Masson 200 times of the CTR group rats, I is the heart muscle HE400 times of the NDCM group rats, J is the heart muscle Masson 200 times of the NDCM group rats, K is the heart muscle HE400 times of the DCM group rats, L is the heart muscle Masson 200 times of the DCM group rats, and M is the myocardial collagen area fraction in the heart muscle cells of each group of rats.

phosphate pathway, folate biosynthesis, galactose metabolism, biosynthesis of amino acids, valine, leucine and isoleucine biosynthesis, phenylalanine, tyrosine and tryptophan biosynthesis, and metabolic pathways.

Several related metabolic pathways were identified as relevant based on the differential metabolites that were identified from the NDCM group compared to the CTR group. As illustrated (Fig. 6C, D), the disorganized metabolic pathways include protein digestion and absorption, cysteine and methionine metabolism,

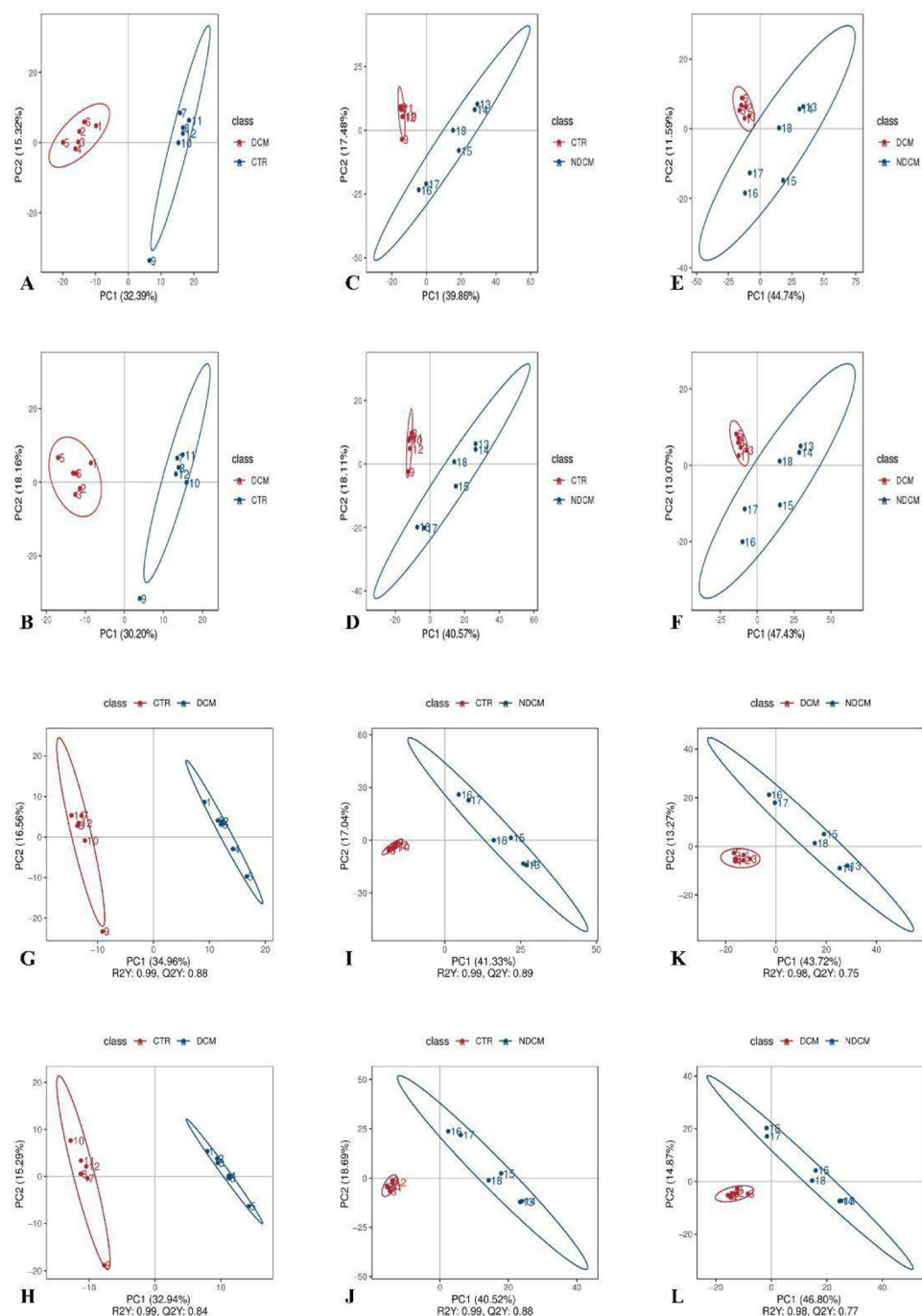


Fig. 4. The horizontal axis PC1 and vertical axis PC2 in the figure represent the scores of the first and second-ranked principal components, respectively. Different coloured scatter points represent samples from different experimental groups, and the ellipse is the 95% confidence interval (when the number of biological replicates is less than 4, the 95% confidence ellipse cannot be displayed). PCA analysis of serum metabolomics in each group of rats is shown in the figure. Among them, A and B are the POS and NEG modes of DCM. vs. CTR, C and D are the POS and NEG modes of NDCM. vs. CTR, E and F are the POS and NEG modes of DCM. vs. NDCM, respectively. OPLS-DA analysis of serum metabolomics in each group of rats is also shown in the figure. Among them, G and H are the POS and NEG modes of DCM. vs. CTR, I and J are the POS and NEG modes of NDCM. vs. CTR, K and L are the POS and NEG modes of DCM. vs. NDCM, respectively.

phenylalanine, tyrosine and tryptophan biosynthesis, tryptophan metabolism, glycine, serine and threonine metabolism, biosynthesis of amino acids, ABC transporters, arginine and proline metabolism, and aldosterone synthesis and secretion.

Several related metabolic pathways were identified as relevant based on the differential metabolites that were identified from the DCM group compared to the NDCM group. As illustrated (Fig. 6E, F), the disorganized

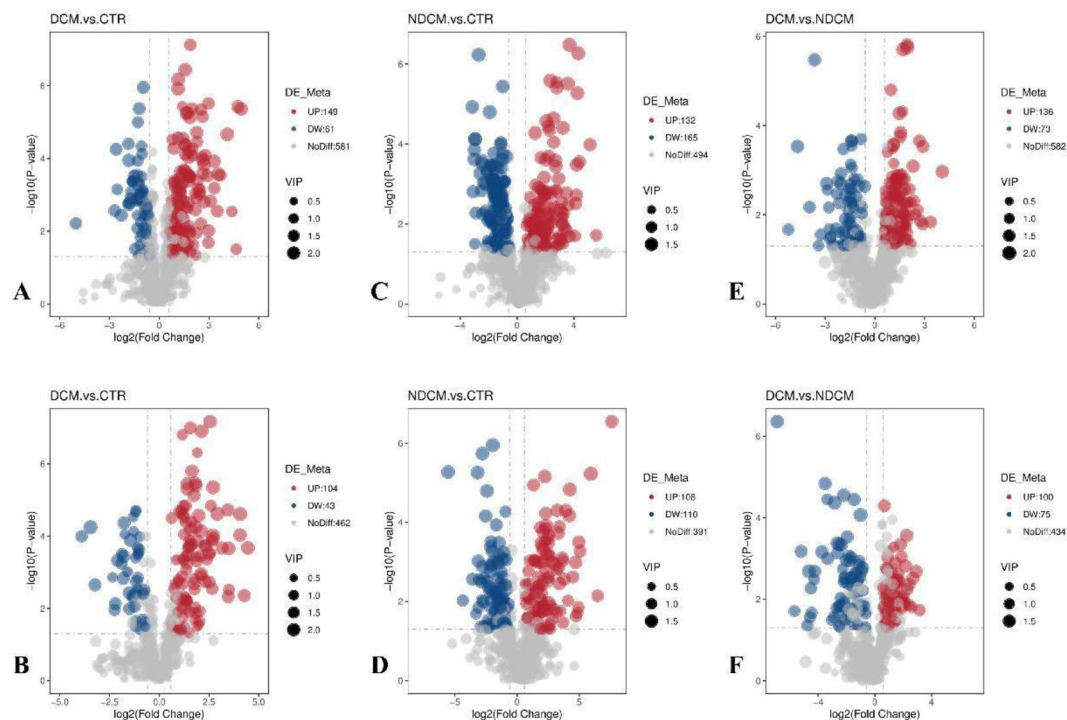


Fig. 5. The volcano plot of differential metabolites in the serum of each group of rats is shown in the figure. Among them, A and B are the POS and NEG modes of DCM. vs. CTR, C and D are the POS and NEG modes of NDCM. vs. CTR, E and F are the POS and NEG modes of DCM. vs. NDCM, respectively.

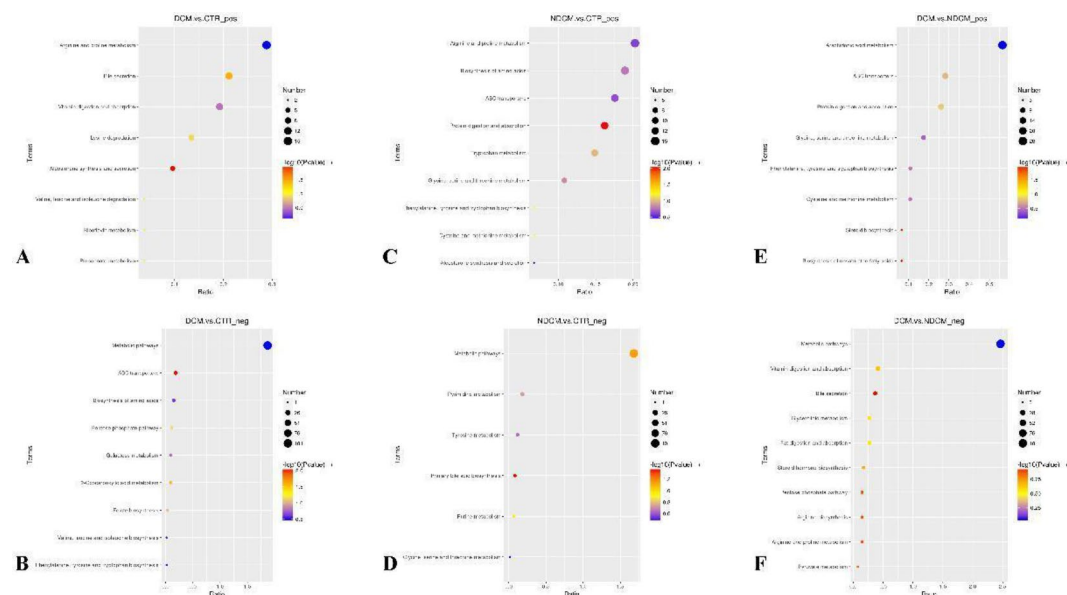


Fig. 6. The KEGG bubble plots of differential metabolites in the serum of each group of rats are shown in the figure. Among them, A and B are the POS and NEG modes of DCM. vs. CTR, C and D are the POS and NEG modes of NDCM. vs. CTR, E and F are the POS and NEG modes of DCM. vs. NDCM, respectively.

metabolic pathways include steroid biosynthesis, steroid hormone biosynthesis, protein digestion and absorption, ABC transporters, cysteine and methionine metabolism, phenylalanine, tyrosine, and tryptophan biosynthesis, glycine, serine, and threonine metabolism, arachidonic acid metabolism, bile secretion, pyruvate metabolism, pentose phosphate pathway, arginine biosynthesis, arginine and proline metabolism, steroid hormone biosynthesis, vitamin digestion and absorption, glycerolipid metabolism, fat digestion and absorption, and metabolic pathways.

In the comparison of the three groups, three differential metabolites were identified in POS mode and four differential metabolites were identified in NEG mode. All the above results are displayed in the form of a Wayne diagram (Fig. 7A, B).

In comparing the three groups, three differential metabolites were identified in POS mode namely 1,7-bis(4-hydroxyphenyl)-5-methoxyheptan-3-one, 5-OxoETE, RNK. And in the comparison of the three groups, four differential metabolites were identified in NEG mode namely Hexadecanedioic acid, PC O-16:4_3:0, D-(-)-Glutamine, 23-Nordeoxycholic acid. The trends of the seven metabolites in the three groups of DCM, CTR, and NDCM are illustrated in box plots (Fig. 7C, D, E, F, G, H, I).

In a bid to find the best biomarkers or panel of biomarkers for the diagnosis of Diabetic Cardiomyopathy ones with the ability to discriminate the DCM from NDCM and CTR, we subjected the individual differential metabolites or combinations of the same to ROC analysis. 5-OxoETE and D-Glutamine the best diagnostic abilities in terms of the AUC for all cross-comparisons. Holistically, the AUC of 5-OxoETE in DCM. vs. CTR was 0.972, in DCM. vs. NDCM was 1.00 and in NDCM. vs. CTR was 1.00. The AUC of D-Glutamine in DCM. vs. CTR was 0.917, in DCM. vs. NDCM was 1.00 and in NDCM. vs. CTR was 1.00. As illustrated in the accompanying (Fig. 8).

Discussion

Diabetic cardiomyopathy refers to the specific cardiomyopathy caused by long-term diabetes independent of hypertension, coronary heart disease and other diseases, and is one of the main causes of death in diabetic patients, especially type 2 diabetes. Based on myocardial cell apoptosis, metabolic disorders, and microvascular disease, this disease leads to extensive focal necrosis of the myocardium and subclinical cardiac dysfunction. It ultimately progresses to heart failure, arrhythmia, and cardiogenic shock, with severe cases even resulting in sudden death.

To study serum biomarkers and related metabolic pathways in diabetic cardiomyopathy, we established a rat model of the condition, which was evaluated using a range of biomarkers and indices, including body weight, diet, water intake, 24-hour urine output, fasting blood glucose, Glycosylated hemoglobin, insulin resistance index, blood lipids, cardiac echocardiography, and histopathology. Untargeted metabolomics is an unbiased metabolomics analysis method aimed at comprehensively detecting and analyzing all metabolites in biological samples to reveal the metabolic network and regulatory mechanisms of the organism. In this study,

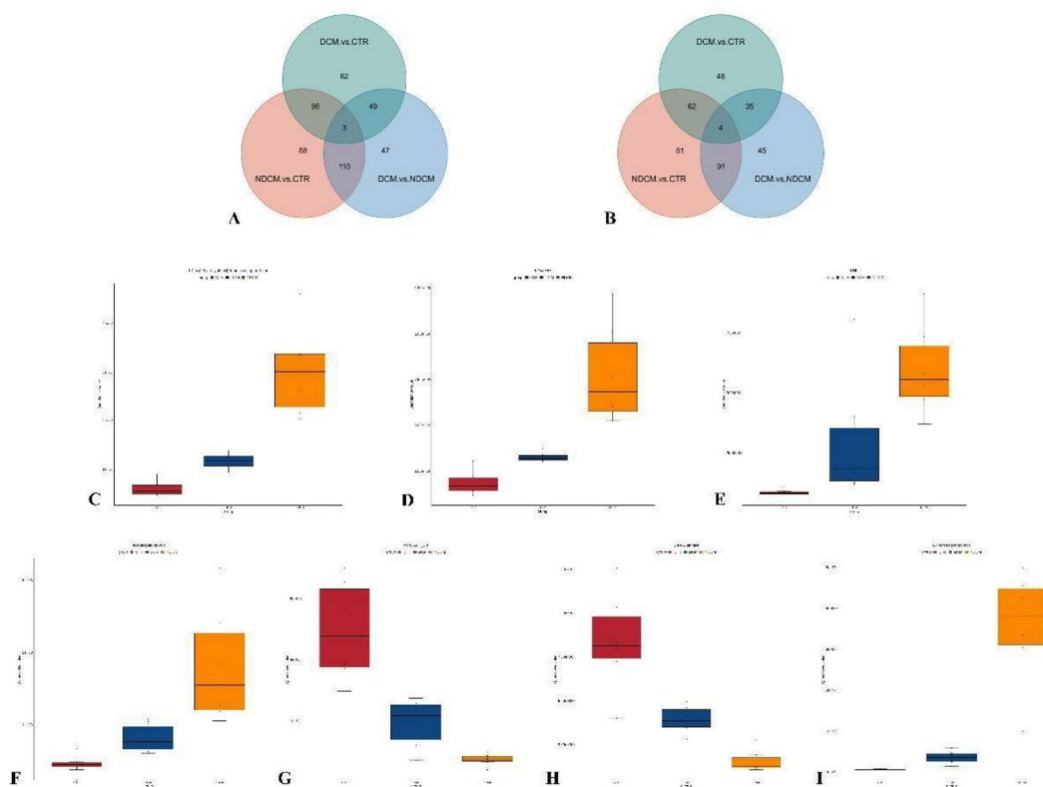


Fig. 7. The differential metabolites in the serum of each group of rats are shown in a Wayne diagram. Among them, A is the serum differential metabolite identified by three groups of rats in POS mode, and B is the serum differential metabolite identified by three groups of rats in NEG mode. The box plots of 7 differential metabolites are also shown in the figure. Among them, C is 1,7-bis(4-hydroxyphenyl)-5-methoxyheptan-3-one, D is 5-OxoETE, E is RNK, F is Hexadecanedioic acid, G is PC O-16:4_3:0, H is D-(-)-Glutamine, I is 23-Nordeoxycholic acid.

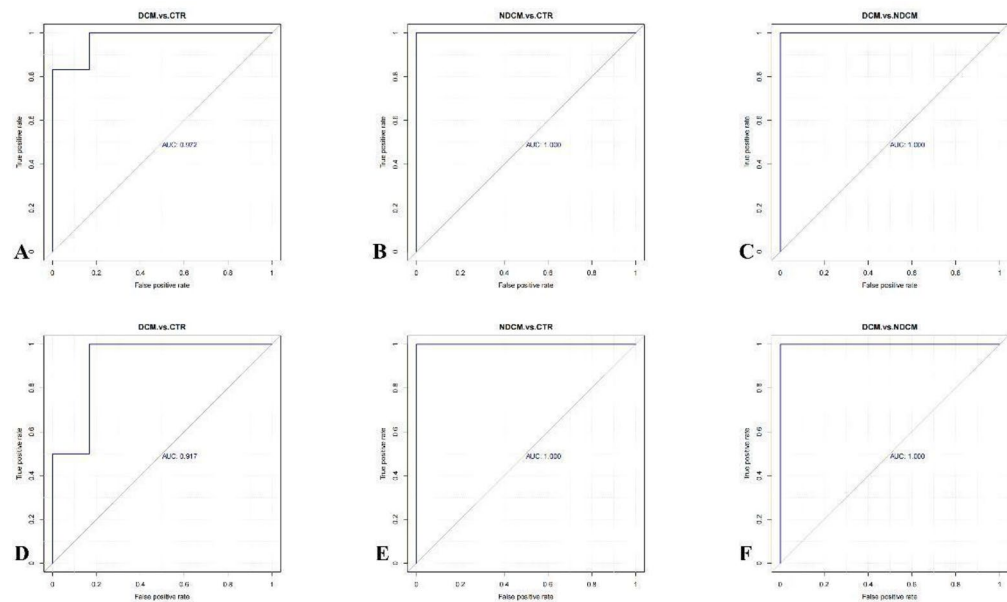


Fig. 8. The ROC curve analysis results of 5-OxoETE and D-Glutamine are shown in the figure. Among them, A, B, and C are the ROC curve analysis results of 5-OxoETE in DCM. vs. CTR, NDCM. vs. CTR, and DCM. vs. NDCM, respectively. D, E and F are the ROC curve analysis results of D-Glutamine in DCM. vs. CTR, NDCM. vs. CTR, and DCM. vs. NDCM, respectively.

we used non-targeted metabolomics techniques to investigate the differences in metabolic profiles among the CTR group, DCM group, and NDCM group. Through multiple cross-comparisons, seven differential metabolites were identified, namely Hexadecanedioic acid, PC O-16:4_3:0, D-Glutamine, 23-Nordeoxycholic acid, 1,7-bis(4-hydroxyphenyl)-5-methoxyheptan-3-one, 5-OxoETE and RNK. Among them, 5-OxoETE and D-Glutamine, two metabolites, show promising diagnostic potential. Our cross-comparison revealed that the potential metabolic pathways associated with these differential metabolites are mainly related to arachidonic acid metabolism and amino acid metabolism, with particular emphasis on the involvement of 5-OxoETE and D-Glutamine. Our results emphasize the importance of these metabolites and their related pathways in the pathophysiology of diabetic cardiomyopathy. They provide new insights for future research on this disease.

5-OxoETE is a product of the arachidonic acid (AA)-dependent 5-lipoxygenase (5-LOX) metabolic pathway²⁸. Studies have shown that inflammation is a central mechanism in the pathophysiology of heart failure with preserved ejection fraction (HFpEF)²⁹. At the same time, myocardial fibrosis is the core mechanism in the pathophysiology of diabetic cardiomyopathy (DCM)⁹. Previous research has demonstrated that in acute myocardial infarction (AMI), the level of 5-oxo-EETE in mouse serum increases and can trigger myocardial injury³⁰. In studies on the rhythmic regulatory mechanisms of mouse cardiomyocytes, an inflammatory response is observed in the early stages of the disease, characterized by elevated levels of pro-inflammatory cytokines; in later stages, due to impaired defense mechanisms for resolving inflammation and exacerbated myocardial fibrosis, the levels of 5-LOX, COX-2, and HO-1 decrease³¹. The present study found that the levels of 5-oxo-EETE in both the diabetic cardiomyopathy (DCM) group and the non-diabetic cardiomyopathy (NDCM) group were significantly elevated compared to the control group (CTR), and the level of 5-oxo-EETE was significantly higher in the NDCM group than in the DCM group. This may be because the NDCM group (with an ejection fraction greater than 50%) mimics the early to mid-stage of HFpEF in cardiomyopathy injury, while the diabetic cardiomyopathy (DCM) group simulates the end-stage of cardiomyopathy or heart failure with reduced ejection fraction (HFrEF).

D-glutamine is the most common and widely used amino acid in the body, playing a crucial role in various physiological processes. It can play a key role as an energy substrate in cell proliferation, antioxidant, and anti-inflammatory properties. At the same time, it also participates in the hexosamine pathway and can alleviate insulin resistance. Glutamine metabolic dysfunction (Gln) is the cornerstone of cardiomyopathy pathology and has been recognized as a key factor in the development of diabetic cardiomyopathy (DCM)³². Research has shown that Gln can improve the outcomes of DCM by alleviating oxidative stress³³, reducing inflammation³⁴, and preventing iron-induced cell death³⁵. In addition, it has been shown to reduce O-GlcNAc levels^{36,37}, which is related to the pathogenesis of DCM. On the contrary, some studies suggest that under different physiological conditions or when Gln metabolism is excessive, Gln may stimulate inflammatory responses by activating T cells or increasing ROS levels, leading to iron-induced cell death³⁵. In our study, we found that D-Glutamine levels were significantly lower in the DCM and non-diabetic cardiomyopathy (NDCM) groups than in the control group (CTR). It is worth noting that the D-Glutamine levels in the DCM group were significantly higher than those in the NDCM group. The receiver operating characteristic (ROC) curves of D-Glutamine were impressive, with AUC values of 0.917, 1.00, and 1.00 for DCM and CTR, DCM and NDCM, and NDCM and

CTR, respectively. These findings suggest that D-Glutamine can serve as a valuable biomarker for the diagnosis and treatment of DCM³⁸.

Our study, however, has several limitations that need to be addressed in future studies to confirm or otherwise our findings. First, as a single-centre study, the sample size is small and could therefore have influenced the outcome of this study, particularly the robustness of the statistical analysis. Second, in addition to LC-MS/MS analysis, other analytical platforms such as (GC-MS, and LC-NMR) can be employed to validate the applicability of these serum biomarkers for diagnostic purposes. Finally, because of the insufficient sample size, we are unable to perform relevant validation on the detected metabolites.

Conclusions

In this study, we established a DCM rat model and conducted serum metabolomics analysis. We identified seven differential metabolites, including Hexadecanedioic acid, PC O-16:4_3:0, D-Glutamine, 23-Nordeoxycholic acid, 1,7-bis(4-hydroxyphenyl)-5-methoxyheptan-3-one, 5-OxoETE and RNK. Of these, two metabolites, namely 5-OxoETE and D-Glutamine, were identified as serum biomarkers for DCM, with involvement in arachidonic acid metabolism and amino acid metabolism.

Data availability

The datasets used and/or analysed during the current study are available from the first author upon reasonable request.

Received: 17 October 2024; Accepted: 14 April 2025

Published online: 28 May 2025

References

1. Saeedi, P. et al. Global and regional diabetes prevalence estimates for 2019 and projections for 2030 and 2045: results from the international diabetes federation diabetes atlas, 9(th) edition. *Diabetes Res. Clin. Pract.* **157**, 107843 (2019).
2. Lorenzo-Almorós, A. et al. *Diabeticcardiomyopathy RevClinEsp (Barc)* **222**(2): 100–111. (2022).
3. Gulsin, G. S. et al. Diabetic cardiomyopathy: prevalence, determinants and potential treatments. *Ther. Adv. Endocrinol. Metab.* **10**, 2042018819834869 (2019).
4. Nakamura, K. et al. Pathophysiology and treatment of diabetic cardiomyopathy and heart failure in patients with diabetes mellitus. *Int. J. Mol. Sci.* **23** (7), 3587 (2022).
5. Dunlay, S. M. et al. Type 2 diabetes mellitus and heart failure: a scientific statement from the American heart association and the heart failure society of America: this statement does not represent an update of the 2017 ACC/AHA/HFSA heart failure guideline update. *Circulation* **140** (7), e294–e324 (2019).
6. Jia, G. et al. Diabetic cardiomyopathy: an update of mechanisms contributing to this clinical entity. *Circul. Res.* **122**, 624–638 (2018).
7. Dia, M. et al. Reduced reticulum-mitochondria Ca transfer is an early and reversible trigger of mitochondrial dysfunctions in diabetic cardiomyopathy. *Basic. Res. Cardiol.* **115** (6), 74 (2020).
8. Conning-Rowland, M. et al. Molecular mechanisms of diabetic heart disease: insights from transcriptomic technologies. *Diab Vasc Dis. Res.* **20** (6), 14791641231205428 (2023).
9. Li, W. et al. Single-cell RNA-seq of heart reveals intercellular communication drivers of myocardial fibrosis in diabetic cardiomyopathy. *Elife* **12**, e80479 (2023).
10. Zhang, X. et al. Impact of inflammation and anti-inflammatory modalities on diabetic cardiomyopathy healing: from fundamental research to therapy. *Int. Immunopharmacol. Oct.* **123**, 110747 (2023).
11. Peng, M. et al. Signaling pathways related to oxidative stress in diabetic cardiomyopathy. *Front. Endocrinol. (Lausanne)*. **13**, 907757 (2022).
12. Nakamura, M. et al. Cardiomyopathy in obesity, insulin resistance and diabetes. *J. Physiol.* **598** (14), 2977–2993 (2020).
13. Jaquenod, D. et al. Ca²⁺ mishandling and mitochondrial dysfunction: a converging road to prediabetic and diabetic cardiomyopathy. *Pflugers Arch.* **474** (1), 33–61 (2022).
14. Hou, J. et al. Pathological roles of oxidative stress in cardiac microvascular injury. *Curr. Probl. Cardiol.* **48** (1), 101399 (2023).
15. Lin, C. Metabolomics for clinical biomarker discovery and therapeutic target identification. *Molecules* **29** (10), 2198 (2024).
16. Qiu, S. et al. Small molecule metabolites: discovery of biomarkers and therapeutic targets. *Signal. Transduct. Target. Ther.* **8** (1), 132 (2023).
17. Jin, Q. et al. Metabolomics in diabetes and diabetic complications: insights from epidemiological studies. *Cells* **10** (11), 2832 (2021).
18. Pereira, P. R. et al. Metabolomics as a tool for the early diagnosis and prognosis of diabetic kidney disease. *Med. Res. Rev.* **42** (4), 1518–1544 (2022).
19. Morze, J. et al. Metabolomics and type 2 diabetes risk: an updated systematic review and Meta-analysis of prospective cohort studies. *Diabetes Care.* **45** (4), 1013–1024 (2022).
20. Zhang, F. et al. Advanced mass Spectrometry-Based biomarker identification for metabolomics of diabetes mellitus and its complications. *Molecules* **29** (11), 2530 (2024).
21. Kolefer, K. et al. Evaluation of Antidiabetic Properties of the Leaves Extract of *Ficus vallis-choudae* Delile in a Model of Type 2 Diabetes Induced by High-Fat Diet and Streptozotocin. *ScientificWorldJournal*. :1502230(2021). (2021).
22. Shawky, L. M. et al. The biological impacts of sitagliptin on the pancreas of a rat model of type 2 diabetes mellitus: drug interactions with Metformin. *Biology (Basel)*. **9** (1), 6 (2019).
23. Zhang, L. et al. Effects of Dapagliflozin monotherapy and combined aerobic exercise on skeletal muscle mitochondrial quality control and insulin resistance in type 2 diabetes mellitus rats. *Biomed. Pharmacother.* **169**, 115852 (2023).
24. Jiang, L. et al. Outcome of patients with coronary artery disease and left ventricular ejection fraction less than 50% undergoing percutaneous coronary intervention. *Zhonghua Xin Xue Guan Bing Za Zhi.* **45** (12), 1058–1066 (2017).
25. Kosaraju, A. et al. Left ventricular ejection fraction. 2023 Apr 24. In *StatPearls [Internet]* (StatPearls Publishing, 2025).
26. Wang, J. et al. Loureirin B reduces insulin resistance and chronic inflammation in a rat model of polycystic ovary syndrome by upregulating GPR120 and activating the LKB1/AMPK signaling pathway. *Int. J. Mol. Sci.* **25** (20), 11146 (2024).
27. Xiao, Z. et al. Ferrostatin-1 alleviates lipopolysaccharide-induced cardiac dysfunction. *Bioengineered* **12** (2), 9367–9376 (2021).
28. Kalyvanaki, K. et al. 5-Oxo-ETE/OXER1: A link between tumor cells and macrophages leading to regulation of migration. *Molecules* **29** (1), 224 (2023).
29. Schiattarella, G. G. et al. Metabolic inflammation in heart failure with preserved ejection fraction. *Cardiovasc. Res.* **117** (2), 423–434 (2021).

30. Lai, Q. et al. Oxoeicosanoid receptor Inhibition alleviates acute myocardial infarction through activation of BCAT1. *Basic. Res. Cardiol.* **116** (1), 3 (2021).
31. Ingle, K. A. et al. Cardiomyocyte-specific Bmal1 deletion in mice triggers diastolic dysfunction, extracellular matrix response, and impaired resolution of inflammation. *Am. J. Physiol. Heart Circ. Physiol.* **309** (11), H1827–H1836 (2015).
32. Durante, W. The emerging role of l-glutamine in cardiovascular health and disease. *Nutrients* **11**, 2092 (2019).
33. Prattichizzo, F. et al. Short-term sustained hyperglycaemia fosters an archetypal senescence-associated secretory phenotype in endothelial cells and macrophages. *Redox Biol.* **15**, 170–181 (2018).
34. Abdullah, C. S. et al. Targeted deletion of T-cell S1P receptor 1 ameliorates cardiac fibrosis in streptozotocin-induced diabetic mice. *FASEB J.* **32**, 5426–5435 (2018).
35. Wang, X. et al. Ferroptosis is essential for diabetic cardiomyopathy and is prevented by Sulforaphane via AMPK/NRF2 pathways. *Acta Pharm. Sin B.* **12**, 708–722 (2022).
36. Masaki, N. et al. O-GlcNAcylation mediates glucose-induced alterations in endothelial cell phenotype in human diabetes mellitus. *J. Am. Heart Assoc.* **9**, e014046 (2020).
37. De Blasio, M. J. et al. Defining the progression of diabetic cardiomyopathy in a mouse model of type 1 diabetes. *Front. Physiol.* **11**, 124 (2020).
38. Ha, K. S. Et al. transglutaminase 2 in diabetes mellitus: unraveling its multifaceted role and therapeutic implications for vascular complications. *Theranostics* **14** (6), 2329–2344 (2024).

Acknowledgements

Dr. Liu Guangliang of Chongqing Medical University Affiliated Second Hospital Jiangnan Branch Chongqing Key Laboratory of Cardiac Electrophysiology, Fu Xingxing of Jiangnan Branch Experimental Animal Center of the Second Affiliated Hospital of Chongqing Medical University, who made available materials and basic equipment to undertake the initial separation and storage of tissue pathology samples and blood samples. We also sincerely wish to thank NovogeneCo Ltd for the technical assistance.

Author contributions

J.L., H.Q. conducted animal experiments. H.Q. did the raw data curation and the formal analysis. Y.W. performed the analysis. J.L., H.Q. wrote the manuscript. S.L. supervised the research. All authors took part in the discussion leading up to the manuscript. All authors read and approved the final manuscript.

Funding

This study was funded by the Chongqing Science and Technology Bureau project (cstc2021jcyj-msxmX0208) and the Guizhou Provincial Science and Technology Plan project (Qianke He [2024] Yiban 360).

Declarations

Competing interests

The authors declare no competing interests.

Ethical consideration

Written informed consent for publication of this paper was obtained from The Institutional Review Board of the Second Affiliated Hospital of Chongqing Medical University.

Additional information

Correspondence and requests for materials should be addressed to L.S.

Reprints and permissions information is available at www.nature.com/reprints.

Publisher's note Springer Nature remains neutral with regard to jurisdictional claims in published maps and institutional affiliations.

Open Access This article is licensed under a Creative Commons Attribution-NonCommercial-NoDerivatives 4.0 International License, which permits any non-commercial use, sharing, distribution and reproduction in any medium or format, as long as you give appropriate credit to the original author(s) and the source, provide a link to the Creative Commons licence, and indicate if you modified the licensed material. You do not have permission under this licence to share adapted material derived from this article or parts of it. The images or other third party material in this article are included in the article's Creative Commons licence, unless indicated otherwise in a credit line to the material. If material is not included in the article's Creative Commons licence and your intended use is not permitted by statutory regulation or exceeds the permitted use, you will need to obtain permission directly from the copyright holder. To view a copy of this licence, visit <http://creativecommons.org/licenses/by-nc-nd/4.0/>.

© The Author(s) 2025